

# X-ray resonant magnetic scattering study of magnetic stripe domains in $\alpha$ -GdFe thin films

J. Miguel,<sup>1,\*</sup> J. F. Peters,<sup>1,†</sup> O. M. Toulemonde,<sup>1,‡</sup> S. S. Dhesi,<sup>2,§</sup> N. B. Brookes,<sup>2</sup> and J. B. Goedkoop<sup>1</sup>  
<sup>1</sup>*Van der Waals-Zeeman Institute, University of Amsterdam, Valckenierstraat 65, 1018 XE, Amsterdam, The Netherlands*  
<sup>2</sup>*European Synchrotron Radiation Facility, ESRF, Boîte Postale 220, F-38043 Grenoble Cedex, France*  
 (Received 10 March 2006; revised manuscript received 12 August 2006; published 29 September 2006)

X-ray resonant magnetic scattering (XRMS) has been used to investigate the structure of magnetic stripe domain patterns in thin amorphous GdFe films. Under the influence of a perpendicular magnetic field, the scattered intensity displays a smooth transition from a structure factor of correlated stripes to the form factor of isolated domains. We derive a quite general expression that relates the total scattered intensity of XRMS to the absolute value of the magnetization. Furthermore, we compare our results for the domain period with domain theory. We obtain good agreement for prealigned stripes, but disorder tends to lead to an overestimation of the period measured with XRMS.

DOI: [10.1103/PhysRevB.74.094437](https://doi.org/10.1103/PhysRevB.74.094437)

PACS number(s): 75.60.Jk, 75.60.Ch, 61.10.Eq, 68.37.Rt

## I. INTRODUCTION

The study of magnetic domains<sup>1</sup> has a long tradition which is kept alive by the importance of domain structure for data storage media. In such devices, as well as in domain walls, the magnetic structure is modulated on the nanometer length scale. New techniques that exploit the strong magneto-optical contrast at certain x-ray absorption transitions are making strong contributions to magnetic structure research: transmission x-ray microscopy (TXM)<sup>2-4</sup> and photoelectron emission microscopy (PEEM)<sup>5-8</sup> are now able to image magnetic structures with resolutions in the 10 nm range. X-ray resonant magnetic scattering (XRMS),<sup>9-25</sup> on the other hand, probes the magnetic structure in Fourier space and provides the ensemble averaged properties of the magnetic structure. In this paper we discuss new aspects of x-ray resonant magnetic scattering in a detailed analysis of data on the evolution of stripe domains in amorphous GdFe films under perpendicularly applied magnetic fields.

Stripe domains are meandering domain patterns found in thin films displaying perpendicular anisotropy (PMA),<sup>11,26-33</sup> in which the magnetization self-organizes in alternating up and down magnetized bands. They result from the competition between the local exchange and anisotropy interactions that favor a single saturated domain state with the long-ranged demagnetizing dipolar field that tends to break up this single domain, at the cost of the creation of domain walls. Given the right combination of thickness and magnetic properties, highly correlated up and down domains form, as shown schematically in Fig. 1(a).

In their seminal work on stripe domains, Kooy and Enz<sup>26</sup> found accurate expressions for the width of the up and down domains in perpendicular fields, assuming infinitely thin domain walls. However, when the film thickness is comparable to the domain period, the structure of the domain wall has to be considered. Thus, closure domains can form, further minimizing the dipolar energy<sup>34</sup> and altering the domain wall energy [Fig. 1(b)]. To some extent, these effects have been incorporated in extensions of the Kooy and Enz model.<sup>28,30-32,35</sup> Alternatively, the true domain structure can be calculated accurately using micromagnetic finite element methods,<sup>29,36,37</sup> which, however, require the stripe period as

an input parameter. Given this situation, high resolution experimental data are required to further test these models.

The amorphous GdFe films<sup>38,39</sup> studied here belong to the same family as amorphous TbFeCo films used in magnetic recording.<sup>40</sup> They have a highly disordered atomic structure, but are very homogeneous and defect free on a length scale larger than a few nanometers, implying a flat domain wall pinning energy landscape.<sup>40</sup> In our samples, this is reflected in a particularly high degree of perfection in the alignment of the stripe systems that form after in-plane magnetic saturation.

Two films are compared here that differ slightly in composition but have a quite different domain width and magnetization loop. We discuss the differences in evolution starting from either aligned or disordered initial stripe structures. Furthermore, we discuss the strong circular dichroism in the scattering of the aligned domain lattice. This analysis results

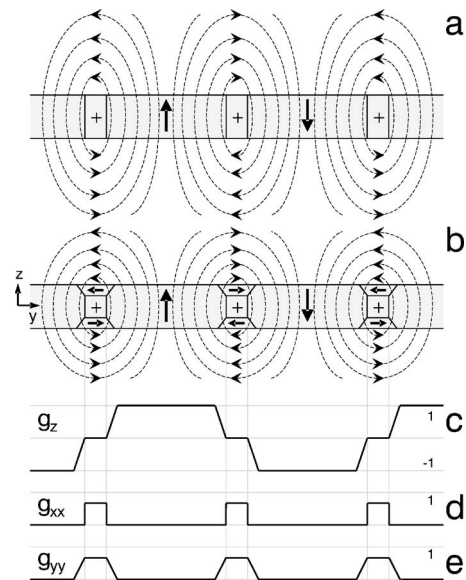


FIG. 1. A schematic representation of stripe domains (a) without and (b) with closure domains. In reality, the magnetization forms a continuous three-dimensional structure. (c), (d), and (e) The contrast functions as seen by an x-ray beam traversing the film (see Sec. IV A).

TABLE I. Magnetic properties of the  $\text{Gd}_{1-x}\text{Fe}_x$  films. The quantities to the right of the vertical line are discussed in Sec. IV E.

Sample	$x$ (% Fe)	$M_s$ (kA/m)	$K_u$ ( $10^5$ J/m $^3$ )									
				$Q$	$\mu^*$	$\chi_r^0$	$l_c$ (nm)	$\gamma_w$ ( $10^{-4}$ J/m $^2$ )	$\delta$ (nm)	$A$ ( $10^{-12}$ J/m)	$\lambda_c$	
A	0.83	221	0.18	0.58	2.73	2.5	13.9	8.5	37.2	2.6	0.33	
B	0.81	150	0.17	1.21	1.82	12.3	33.2	9.3	42.9	3.2	0.79	

in a method of obtaining the magnetization directly from the scattering curves, which turns out to work well for the disordered stripe systems. Furthermore, we point out a general relation between the total scattered intensity and the absolute value of the magnetization. Finally, we find that the domain size of the aligned case is described quite well by a domain theory model,<sup>31</sup> in contrast to the disordered cases.

## II. EXPERIMENTAL

$\text{Gd}_{1-x}\text{Fe}_x$  magnetic thin films with  $x=0.83$  (sample A) and  $0.81$  (sample B) were grown by electron beam coevaporation on a rotating sample holder at  $1 \times 10^{-9}$  mbar. A thickness of 42 nm was chosen to give approximately  $1/e$  absorption at the Gd  $M_5$  resonance energy using the calculated cross sections by Thole *et al.*<sup>41</sup> As supports we used 100 nm thick  $\text{Si}_3\text{N}_4$  windows, which have a transmission of  $\sim 95\%$  at the Gd  $M_5$  resonance energy. The magnetic films were capped with a 2 nm thick Al protection layer in order to prevent oxidation. X-ray diffraction scans showed no trace of structural order in the GdFe films. Rutherford back scattering was used to determine the film thicknesses, as well as to check the composition and homogeneity. Atomic force microscopy (AFM) measurements showed that the surfaces were free of pinholes and were flat and structureless on the 1 nm scale.

The values of saturation magnetization  $M_s$  and anisotropy constant  $K_u$  as determined with vibrating sample magnetometer (VSM) are summarized in Table I. The main distinction between the samples is the 33% smaller saturation magnetization of sample B due to it being closer to the room-temperature ferrimagnetic compensation composition  $x_c \approx 0.76$ .<sup>38</sup>

The x-ray experiments reported here were carried out at the soft x-ray beamline ID08 at the European Synchrotron Radiation Facility.<sup>42</sup> Figure 2 schematically shows the employed experimental setup. The Apple II undulator source offers complete control over the polarization. The experiments were performed with modest energy resolution  $\Delta E/E \leq 10^{-3}$  and a beam size of  $100 \mu\text{m}$ . The sample was mounted in a room-temperature rotatable holder, allowing us to preset the initial alignment of the stripe lattice to an ordered or disordered lattice by saturating the sample in plane or out of plane, respectively.

The incident intensity  $I_0$  was monitored by reading the drain current from the refocusing mirror. As a detector we used a P20 phosphor-coated ( $5 \mu\text{m}$  thick,  $1 \mu\text{m}$  grain size) vacuum window with a 12-bit charge-coupled device (CCD) camera. For the present experiments, a TV lens combined with a 5 mm macroring was used, giving a field of view of  $\sim 15$  mm and a  $10 \mu\text{m}$  resolution.

## III. RESULTS

### A. Scattering curves at remanence

In the absence of an applied field, both samples have vanishing magnetization. Typical domain morphologies found in the remanent state are depicted in the left column of Fig. 3. After out-of-plane magnetic saturation, both samples have completely disordered, meandering patterns with appreciable domain branching and truncation [Figs. 3(a) and 3(c)]. In-plane saturation, on the other hand, leads to the appearance of a highly aligned quasi-one-dimensional domain lattice [Fig. 3(b)].

It should be noted that these magnetic force microscopy (MFM) images are affected to some extent by tip-domain interactions, visible as a horizontal discontinuity observable in the center image. We found that stable images appear typically only after a few sweeps over the field of view even when using low-moment tips, indicating low domain wall pinning. On the other hand, the aligned stripe system [Fig. 3(b)] is much more stable and shows a remarkably perfect grating structure. The stripe periods as obtained from MFM are listed in Table II.

On the right of the MFM images in Fig. 3 we show details of the corresponding two-dimensional (2D) XRMS diffraction patterns. The beam stops were either a horizontal 1 mm thick Cu wire [sample A, Figs. 3(d) and 3(e)] or a knife edge [sample B, Fig. 3(f)], giving scattering vector ranges of (0.004–0.05) and (0.01–0.20)  $\text{nm}^{-1}$ , respectively. The diffuse background was eliminated before further data processing by subtracting exposures taken at magnetic saturation. The disordered stripe patterns produce a broad ring of scattered intensity while the aligned stripe system produces very sharp and intense peaks which at the Gd  $M_5$  resonance con-

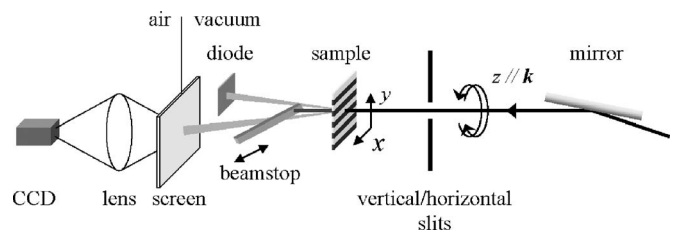


FIG. 2. Schematic representation of the experimental setup. From right to left, the left or right circularly polarized x-ray beam, after being reflected by the refocusing mirror, is cleaned by vertical and horizontal slits. The magnetic domain structure of the sample produces a scattering pattern that can be recorded either by a photodiode or a scintillator screen on the end flange of the vacuum system. The visible light image is recorded by a CCD camera. A beamstop blocks the primary beam.

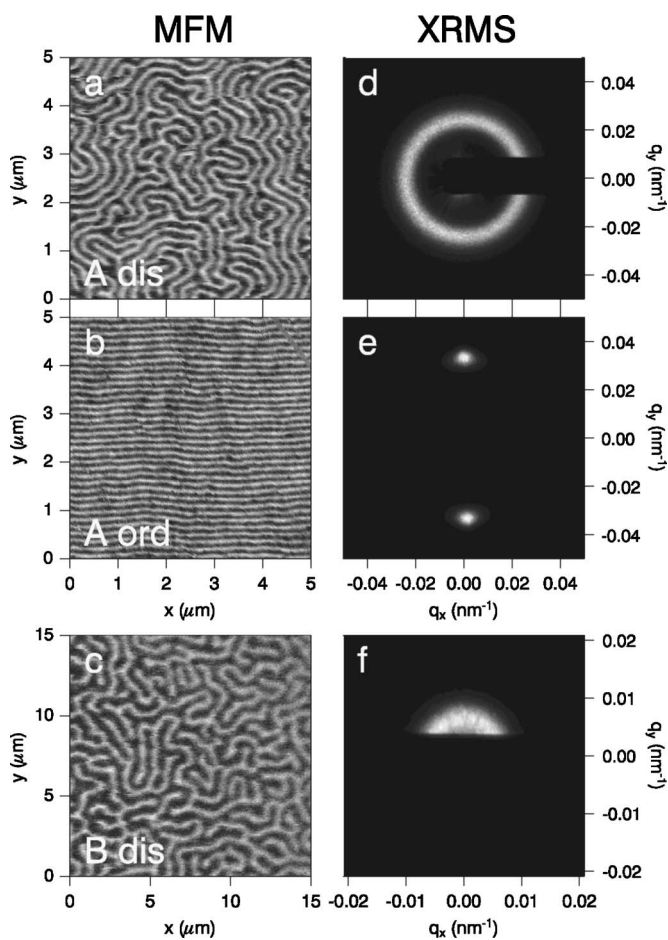


FIG. 3. Left: MFM images of the remanent magnetic domain patterns of sample *A* (83% Fe) after (a) out-of-plane and (b) in-plane magnetization. (c) Domain pattern of sample *B* (81% Fe) after out-of-plane saturation. Right: corresponding measured 2D diffraction patterns.

tain 5% of the transmitted primary beam intensity.<sup>11,43,44</sup>

The angularly integrated diffraction patterns of Figs. 3(d) and 3(f) are given in Fig. 4. The scattered intensity of the disordered stripes in sample *A*, Fig. 4(a) shows clear first and third diffraction orders. The peak position  $q_r$  gives a period of  $\tau = 2\pi/q_r = 253$  nm, about 10% larger than the period obtained from MFM (see Table II). From the full width at half maximum, corrected for the experimental resolution, we obtain a crude estimate for the correlation length  $\xi \approx 524$  nm or two periods.

The ordered lattice prepared by in-plane saturation shows a series of diffraction peaks, five of which are shown in

TABLE II. Stripe periods as obtained from MFM and XRMS, and correlation length-to-period ratio from XRMS.

Sample	$\tau_{\text{(MFM)}}$ (nm)	$\tau_{\text{(XRMS)}}$ (nm)	$\xi/\tau$
<i>A</i> dis	232	253	2
<i>A</i> ord	160	162	8
<i>B</i> dis	835	934	1.2

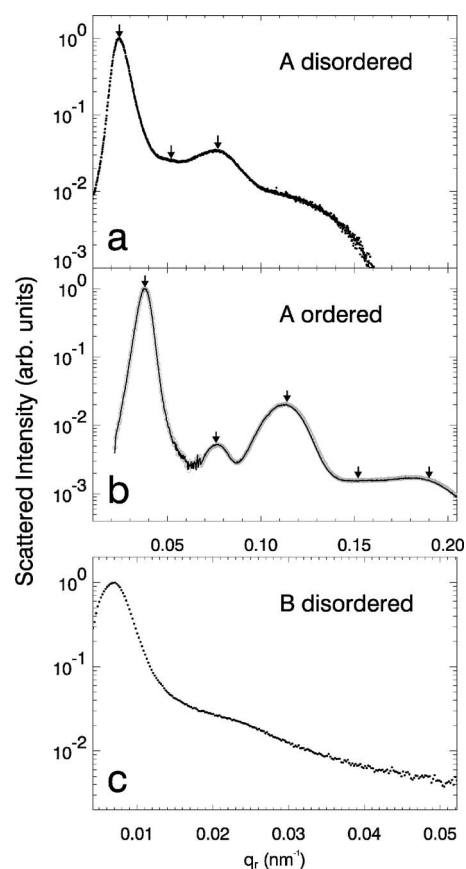


FIG. 4. Scattered intensity obtained by azimuthal integration of the XRMS results as in Fig. 3, taken with left- (line) and right-circular (open symbols) polarization.

Fig. 4(b). The first-order peak corresponds to a period of  $\tau = 162$  nm, agreeing very well with the MFM value, with a correlation length of 1440 nm, more than 8 times the period. The presence of the higher orders clearly indicates that the domain walls are quite sharp in this case. The peak width increases linearly with the diffraction order due to the residual disorder in the stripe lattice.<sup>45</sup>

Finally, sample *B*, Fig. 3(c) only displays a very broad maximum, corresponding to a domain size  $\tau = 934$  nm, approximately 12% larger than the one obtained from MFM and with a correlation length of only 1.2 times the average period.

## B. Field-dependent scattering curves

Figure 5 shows the evolution of the angularly integrated scattered intensity over the magnetization loop for both samples. Also shown is the behavior of sample *A* starting from the aligned case taken with left and right circularly polarized light, and the corresponding dichroic asymmetry. In all cases we observe a clear evolution of peak positions and intensities of the higher orders. At higher fields, the peaks gradually disappear and the spectra develop into broad structures with intensity minima that move to higher  $q$  as the field becomes increasingly positive. In the aligned case the spectra show a characteristic circularly dichroic asymmetry,

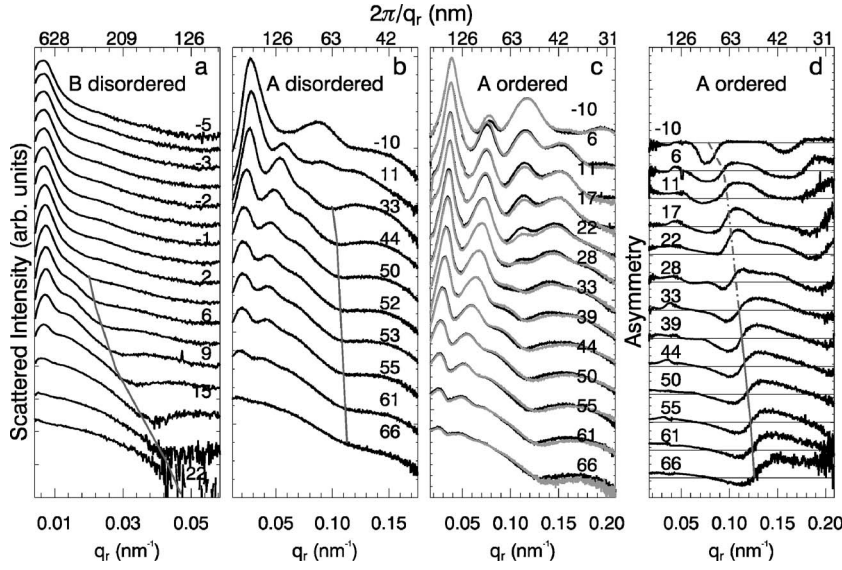


FIG. 5. Field-dependent evolution of the scattered intensity for the disordered domains of samples *B* (a) and *A* (b) and for the aligned stripes in sample *A* (c), taken with left (black) and right (gray) circularly polarized beams. Data are displayed on a logarithmic scale. The asymmetry  $\frac{I_- - I_+}{I_- + I_+}$  for the ordered case of sample *A* is shown using a linear scale in (d). The value of the applied field in mT is shown next to the traces. For the sake of clarity not all curves are shown.

with a zero crossing located at the intensity minima.

Figure 6 shows the information that can be extracted from the complete data set: (a) the normalized perpendicular magnetization loops for the two samples, (b) the domain period  $\tau$ , (c) the width of the reversed domain  $w_d$ , (d) the correlation length normalized to the period  $\xi/\tau$ , and (e) the total scattered intensity. The angular distribution of the scattered intensity was constant for the three cases:  $360^\circ$  for the disordered cases and  $5^\circ$  for the aligned case (sample *A*).

## IV. DISCUSSION

### A. Stripe diffraction patterns in the small-angle limit

We will first discuss the case of the aligned stripe systems present in sample *A* after in-plane magnetization. We will initially neglect the remaining disorder and approximate it by a perfectly periodic structure of period  $\tau$  in the  $\hat{y}$  direction, taking the stripe magnetization along the  $\hat{z}$  direction (coordinate system as defined in Fig. 2). In order not to lose generality we allow that the Bloch walls, magnetized along the  $\hat{x}$  direction, are dressed with closure caps with magnetization along the  $\pm\hat{y}$  direction.

In resonant magnetic scattering one has to take into account the polarization of the light and the tensorial nature of the scattering cross section.<sup>9,15</sup> Hill and McMorrow<sup>46</sup> wrote the atomic scattering tensor as a Jones matrix that describes the scattering of the incident electric field  $\mathbf{E}_0 = E_0(\epsilon_x, \epsilon_y)$  into an outgoing field  $\mathbf{E} = E(\epsilon'_x, \epsilon'_y)$ . In the small-angle scattering limit, which is applicable in this work because the domain size is at least 150 times the wavelength, the magnetization-dependent part of the Jones matrix of an atom with magnetization pointing along the unit vector  $\mathbf{m}$  in a beam incident along the  $\hat{z}$  axis reduces to

$$\mathcal{F}(\omega) = \begin{pmatrix} 0 & -im_z \\ im_z & 0 \end{pmatrix} F^{(1)} + \begin{pmatrix} m_x^2 & m_x m_y \\ m_x m_y & m_y^2 \end{pmatrix} F^{(2)}. \quad (1)$$

The two terms, with energy-dependent scattering amplitude  $F^{(1)}(\omega)$  and  $F^{(2)}(\omega)$ , include either only the out-of-plane

component  $m_z$  or the in-plane components  $m_x$  and  $m_y$ . If the film is homogeneously magnetized out of plane (in plane), the imaginary parts lead, respectively, to circular (linear) dichroism in the absorption. In a separate study we have performed absolute absorption measurements of the Gd  $M_{4,5}$  spectra, corresponding to the imaginary parts of  $F^{(i)}$ , from which the real parts were derived, using the Kramers-Kronig transform.<sup>47</sup> At the photon energy used here ( $E = 1184$  eV),  $|F^{(2)}/F^{(1)}|^2 = 0.164$ .

A nonuniform magnetization  $\mathbf{m}(\mathbf{r})$  produces a scattered wave amplitude  $\mathbf{E}(\mathbf{q})$  which is proportional to the Fourier transform of Eq. (1) over the sample volume. The Fourier integral over the sample thickness leads to a total phase shift and absorption at each position  $y$ , depending on the contrast functions  $g_z(y) = \int_{-t/2}^{t/2} m_z(y, z) dz$  and  $g_{ij}(y) = \int_{-t/2}^{t/2} m_i(y, z) m_j(y, z) dz$  ( $i, j = x, y$ ), where  $t$  is the film thickness. Since the Bloch wall magnetization  $m_x$  is symmetric with respect to the film midplane, while the closure domain magnetization  $m_y$  is antisymmetric, the contrast function  $g_{xy}(y)$  vanishes. Examples of the three remaining contrast functions are given in Fig. 1.

Since the structure is invariant along the  $\hat{x}$  direction, the Fourier transform in this direction yields a trivial delta function  $\delta(q_x)$ . The remaining Fourier transform along  $\hat{y}$  gives the outgoing field amplitude at scattering wave vector  $q_y$ ,

$$\mathbf{E}(q_y) = \left[ \begin{pmatrix} 0 & -iG_z \\ iG_z & 0 \end{pmatrix} F^{(1)} + \begin{pmatrix} G_{xx} & 0 \\ 0 & G_{yy} \end{pmatrix} F^{(2)} \right] \mathbf{E}_0, \quad (2)$$

where  $G_z(q_y)$ ,  $G_{xx}(q_y)$  and  $G_{yy}(q_y)$  are the Fourier transforms of the corresponding contrast functions.

The scattered intensity is the absolute square of this amplitude. In particular, for circularly polarized incident light  $\mathbf{E}_0 = E_0(1, \pm i)$  with helicity  $\pm 1$ , the total intensity has a helicity-dependent term

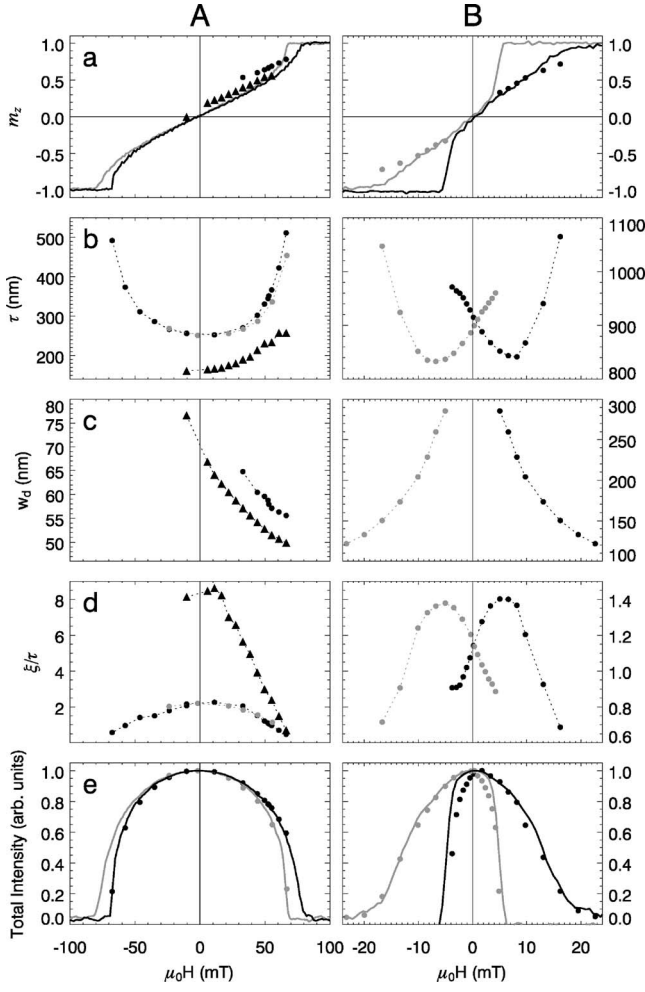


FIG. 6. From top to bottom, (a) the hysteresis loops (full line) together with the magnetization value obtained from the scattering data (symbols), (b) the period  $\tau$ , (c) the reversed domain size,  $w_d$ , estimated from the minima of the form factor, (d) the first-order peak FWHM to period ratio, and (e) the total integrated intensity (symbols), together with the  $1 - \langle m_z \rangle^2$  curves, calculated from the hysteresis loops (full lines). Left panels: sample A, right panels: sample B.  $\bullet$  represents data obtained from the disordered state,  $\blacktriangle$  from the aligned one. Black/gray: increasing/decreasing field.

$$I_{\pm} = I_0 \left\{ |F^{(1)}G_z|^2 + \frac{1}{2} (|F^{(2)}G_{xx}|^2 + |F^{(2)}G_{yy}|^2) \pm \text{Re}[(F^{(1)}G_z)^* F^{(2)}(G_{xx} + G_{yy})] \right\}. \quad (3)$$

The last term is the interference between the polarization-rotating  $F^{(1)}$  term and the polarization-conserving  $F^{(2)}$  term. It can give rise to circular dichroism in the scattered intensity if it is nonzero, which happens when  $m_z(y)$  has the same spatial frequencies as  $m_x^2(y)$  or  $m_y^2(y)$ . The resulting asymmetry is

$$\frac{I_+ - I_-}{I_+ + I_-} = \frac{\text{Re}[(F^{(1)}G_z)^* F^{(2)}(G_{xx} + G_{yy})]}{|F^{(1)}G_z|^2 + \frac{1}{2} (|F^{(2)}G_{xx}|^2 + |F^{(2)}G_{yy}|^2)}. \quad (4)$$

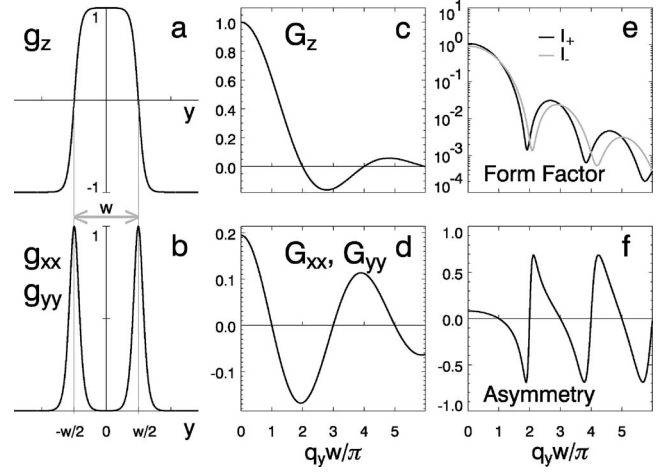


FIG. 7. Generic real space scattering contrast functions for (a) a single up domain and (b) an in-plane (Bloch or closure) magnetization component. Panels (c), (d) show respectively their Fourier transforms. Corresponding form factor for circular- and linear-polarized light for  $|F^{(2)}/F^{(1)}|^2 = 0.164$  ( $\hbar\omega = 1184$  eV) (Ref. 47) are shown in (e) and the asymmetry ratio  $I_+ - I_- / I_+ + I_-$  in (f). The domain wall to domain width ratio is 2:9.

With these results we can explain the scattering curves of Figs. 5(c) and 5(d). The Fourier transform of the periodic  $m_z$  magnetization,  $G_z(q_y)$ , will have maxima at  $q_y = 2\pi n/\tau$  with  $n$  any integer, where the total period  $\tau = w_u + w_d$  is the sum of the up- and down-domain widths  $w_u$  and  $w_d$ . However, we see from Fig. 6(a) that at remanence  $\langle m_z \rangle = 0$  and therefore  $w_u = w_d = \tau/2$ . In this case the only non-zero terms of  $G_z(q_y)$  are at  $q_y = 2\pi n/\tau$  with  $n$  odd. On the other hand, since the period of  $m_x^2$  and  $m_y^2$  is half that of  $m_z$ ,  $G_{xx}(q_y)$  and  $G_{yy}(q_y)$  are non-zero only at  $q_y = 2\pi n/\tau$  with  $n$  even. We see that at remanence, the odd order diffraction peaks are produced only by the out-of-plane magnetization component, while the even order peaks are due to the in-plane magnetization components in the Bloch wall and the closure domains. As a result of this particular situation, the last term of Eq. (3) vanishes, explaining the absence of dichroism in the remanent scattering curves of Fig. 4. For finite magnetization,  $G_z(q_y)$  contains terms with any integer  $n$ , which will interfere with  $G_{xx}(q_y)$  and  $G_{yy}(q_y)$ , giving rise to the dichroic asymmetry observed in sample A in the ordered case [Fig. 5(d)].

The other extreme case that we will discuss is that of an individual down domain (magnetization opposite to the field). In Figs. 7(a) and 7(b) we give a fairly realistic magnetization profile for such a stripe domain, flanked by in-plane domain wall and closure contributions, using a  $\tanh(y)$  function for the domain wall profiles and a wall to domain width ratio of 2:9. The corresponding contrast factors are shown in panels (c) and (d). Inserting these in Eqs. (3) and (4), we obtain the single stripe form factor and asymmetry as shown in Figs. 7(e) and 7(f). These curves resemble closely the high field data at the bottom of Figs. 5(c) and 5(d), respectively, indicating that in this field range the intensity is well approximated by the incoherent superposition of the scattered intensity of isolated stripes. It should be noted here that the minima of the form factor and the zero crossings of

the asymmetry curves are positioned at  $2\pi/w_d$  and therefore provide a simple means to determine the average size of the reversed domains.

### B. Interpretation of scattering curves

In order to interpret the field dependence, we recapitulate briefly the work of Kooy and Enz,<sup>26</sup> who found that the hysteresis loop of magnetic stripe systems has a reversible part at low fields, characterized by reversible adjustments of the domain widths without changes in the overall pattern. This process continues until the reversed domains cannot be compressed more, which happens when they reach a minimum width of about two domain wall widths. From that point on domains are eliminated, causing an increase of the domain period. As a last step, the stripes break up into segments,<sup>32</sup> which gradually shorten to magnetic bubbles that are eventually annihilated by progressively higher fields. On returning from saturation, bubbles nucleate at much lower fields and rapidly finger out to fill the film surface. This difference in annihilation and creation leads to the appearance of a distinctive hysteresis in the magnetization loop, characterized by the triangular shape near magnetic saturation. The main difference between the two samples considered here is the range of the reversible region, which is larger in sample A [see Fig. 6(a)].

We will compare our data with this description starting with the aligned initial state of sample A [Figs. 5(c) and 5(d) and Fig. 6, left]. In the low field reversible region, the diffraction curves show well-defined higher order peaks with an initial correlation length of eight stripes. The system mainly adapts to the field by increasing  $w_u$  with respect to  $w_d$ , while keeping the lattice period more or less constant. This causes the appearance of even orders in the Fourier transform of  $m_z$ , which mix with the scattering of the in-plane components, producing appreciable circular dichroism as discussed above. The angular width (not shown) of the diffraction spots stays constant with the field over the whole field range, indicating that the stripes remain parallel and that we do not reach the bubble state, which should scatter isotropically. However, above  $\sim 20$  mT, the transverse correlation drops linearly with field [see Fig. 6(d), left] to one stripe width, indicating the complete loss of correlation.

The scattering and asymmetry curves become gradually dominated by the form-factor shape of the reversed domains with the intensity minima moving to higher  $q$ . The reverse domain width  $w_d$  estimated from the zero crossing of the dichroic asymmetry [Eq. (4)] is given in Fig. 6(c). It displays a gradual decrease from 78 nm to 50 nm, with a trend to much smaller sizes. This value can be used to estimate the magnetization from the scattering data alone, since for a one-dimensional stripe system the reduced magnetization is equal to  $m \approx w_d/\tau$ . This result is compared with the reduced magnetization in Fig. 6(a), the agreement being quite satisfactory for lower fields, supporting our data interpretation. Clearly, in the bubble regime close to saturation this approach is no longer valid.

By comparing the measured asymmetry curves with a model as in Fig. 7(f), and neglecting possible closure, we

obtain a domain wall width of about 30 nm. With data extending over a more extended range and by using linearly polarized light it should be also possible to get very precise information on the reversed domain and the spin structure of the adjacent Bloch wall and closure magnetization.

### C. The effect of disorder

Although the aligned stripes can be qualitatively described with the one-dimensional lattice model, the finite peak widths indicate the presence of disorder in the stripe lattice. Hellwig *et al.*<sup>13</sup> applied a model<sup>45</sup> to describe moderate disorder in the domain period of the aligned structure. An important result from this model is that disorder causes a shift of the first-order peak towards lower  $q$  values. This implies that the position of the first-order peak tends to overestimate the real domain period. Such an overestimation is the reason for the 10% discrepancy between the MFM and XRMS derived periods for the disordered domain structures given in Table II.

However, actual fitting of the diffraction curves with this model turns out to be possible only in the most ordered case of sample A near remanence. From this fit we obtain a Gaussian distribution in the domain period with a standard deviation equal to 5% of the domain period and a domain wall width of 19 nm, which is much smaller than the 30 nm obtained from the rather crude fit to the high field data.

Fitting with this one-dimensional model becomes impossible for the 2D disordered case of sample A [Fig. 5(b)]. The peak width at remanence corresponds to a correlation length of only two stripes. In applied fields, the diffraction pattern broadens much faster than in the aligned case, and quickly merges in the form factor structure of uncorrelated stripes. The period, correlation length, and scattered intensity, also shown in the left column of Fig. 6 all show quasi-parabolic-field dependence with only a little hysteresis. Compared to the aligned system, the period is always much larger due to imperfections in the lattice, such as branching and end points, which prevent the system from reaching the equilibrium domain period. Also, due to disorder, the circular dichroism is washed out over the whole scattering pattern and becomes too small to be observable. Over a limited range the form factor shape is clear enough to extract a reverse domain size, but the magnetization calculated from this is somewhat too large, probably again due to an underestimation of the period.<sup>13</sup>

Sample B is clearly much more disordered, showing only a single broad diffraction peak over much of the magnetization loop. The average domain distance decreases rapidly down to a minimum at 9 mT and then increases to values that fall beyond our minimum transfer-vector range. The correlation length presents a maximum at 8 mT, but it barely deviates from unity. This behavior might indicate that the magnetization arranges in a collection of domains that look somewhat in between a pure bubble and a stripe domain, as seen by others.<sup>48</sup> Nevertheless, the ratio of period and reversed domain size again produces a quite acceptable estimation of the magnetization in this case [Fig. 6(a), right panel]. Also, in contrast with sample A, the period shows

large hysteresis, implying that the domain pattern is far from equilibrium over the whole loop.

#### D. Field dependence of total scattered intensity

As shown in Fig. 6(e), the normalized total scattered intensity for both samples is approximated very well by the function  $1 - \langle m_z \rangle^2$ , depicted by a line for the two branches (gray and black). The same behavior can be seen in other recent work.<sup>12,44</sup> It can be explained by applying Parseval's theorem to the contrast function  $g_z(y)$ ,

$$\frac{1}{\tau} \int_0^\tau |g_z(y)|^2 dy = \int_{-\infty}^{\infty} |G_z(q_y)|^2 dq_y = \sum_k |G_z^{(k)}|^2, \quad (5)$$

where  $G_z^{(k)}$  is the  $k$ th Fourier coefficient of  $G_z(q_y)$ .  $G_z^{(0)}$  is equal to the average value of the reduced magnetization  $m_z = M_z / M_z^{\text{sat}}$

$$\langle m_z \rangle = \frac{1}{\tau} \int_0^\tau g_z(y) dy = G_z(0). \quad (6)$$

Likewise, the term on the left side of Eq. (5) is the average of the squared reduced magnetization  $\langle m_z^2 \rangle$ . Under the condition that the volume of the in-plane magnetization components is small compared to that of the out-of-plane magnetization this term equals unity. If we finally identify the terms in the summation with  $k \neq 0$  as the integrated scattered intensity, we find that the scattered intensity, normalized to the maximum scattering intensity, obeys

$$\frac{I_{\text{scat}}}{I_{\text{scat,max}}} = 1 - \langle m_z \rangle^2. \quad (7)$$

The result implies that the scattered intensity can be used to measure the absolute value of the magnetization for any sample containing mainly out-of-plane domains.

In Fig. 6(e) the intensity predicted by this expression is compared to the measured intensity. A quite good match is obtained and we have found the same agreement in many other samples. Especially, it is worth noting that the field dependence of the scattered intensity is the same for the disordered and aligned cases of sample A, while the period for the two cases is completely different.

#### E. Domain model analysis

The Kooy and Enz model<sup>26</sup> predicts the field dependence of magnetic stripes in perpendicular fields by treating the demagnetization energy in terms of a Fourier expansion and then minimizing the total free energy to obtain the sample magnetization and domain period at equilibrium. The parameters involved are the saturation magnetization  $M_s$ , the uniaxial anisotropy constant  $K_u$ , the exchange stiffness constant  $A$ , and the film thickness  $t$ . They enter the expressions in the form of two dimensionless parameters. First, the reduced anisotropy material constant  $Q = K_u / K_d = 2K_u / \mu_0 M_s^2$  is the ratio between the anisotropy energy and the demagnetization energy. Second, the reduced characteristic length  $\lambda_c$  is the ratio of the characteristic length  $l_c = \frac{\gamma_w}{2K_d}$  and the film

thickness  $t$ , and is a measure for the domain wall energy  $\gamma_w = 4\sqrt{AK_u}$  in relation to the demagnetization energy.

The model assumes that  $Q \gg 1$ , that the film thickness is at least several times larger than the period at remanence, and that the domain wall width is negligible compared to the domain period. The energy lowering due to the tilting of the magnetization close to the film surface is approximated by introducing an effective rotational permeability  $\mu^* = 1 + \frac{1}{Q}$ .

Gehanno *et al.*<sup>31</sup> extended this model with a better approximation for the demagnetizing energy density in order to make it applicable to films with thickness smaller than the domain period and  $Q \leq 1$ . They obtained analytical expressions for the dependence of the reversible normalized magnetization  $m_z$  and the domain period  $\tau$  on the reduced field  $h = H / \mu_0 M_s$ :

$$m_z(h) = \frac{2}{\pi} \arcsin\left(\frac{\pi}{2} \chi_r^0 h\right), \quad (8)$$

$$\tau(h) = \frac{\pi}{2} t \chi_r^0 \sec\left[\frac{\pi}{2} m_z(h)\right]. \quad (9)$$

The reduced magnetic susceptibility is:

$$\chi_r^0 = \left. \frac{\partial m_z}{\partial h} \right|_{h=0} = \frac{2\sqrt{\mu^*}}{\pi} \exp[\pi\lambda_c + f(r)] \quad (10)$$

where  $f(r)$  is a slowly varying function of  $r = \frac{1}{2}\left(1 + \frac{1}{\sqrt{\mu^*}}\right)$ .

The reduced susceptibility at remanence  $\chi_r^0$  can be obtained from the slope of the out-of-plane magnetization loop (see Table I). By using the obtained value and  $\mu^*$  as input parameters in Eq. (10), we determined the characteristic length  $l_c$ , the domain wall energy density  $\gamma_w = 4\sqrt{AK_u} = 2K_d l_c$ , the domain wall width  $\delta = \pi\sqrt{A/K_u}$ , the exchange constant  $A = \frac{\delta\gamma_w}{4\pi}$ , and the reduced characteristic length  $\lambda_c = l_c/t$  (see Table I). We find that in sample A both  $Q$  and  $\lambda_c$  are two times smaller than in sample B, reflecting the difference in saturation magnetization.

The reversible magnetization and domain period calculated from these equations are compared to the magnetization measured with VSM and x-ray derived periods in Fig. 8. In the case of sample A, the period at remanence is now only four times the thickness, and the correlation length is up to eight periods in this case. Furthermore, the period shows very little hysteresis. Indeed, when magnetizing from the aligned situation, the magnetization and domain period are predicted accurately by the model up to quite high fields. On the one hand, this is proof of the retention of a high degree of alignment up to the field where stripes become unstable with respect to dots. On the other hand, this success proves the suitability of the model to describe systems with the period a few times larger than the film thickness even for very thin films.

As was mentioned before, in sample A the disorder of the stripe lattice causes an increase of the remanent period with a factor 1.5, as compared to the aligned case [Fig. 8(b)]. In our view this is purely caused by the branchings and truncations of the disordered stripe system taking up more space, rather

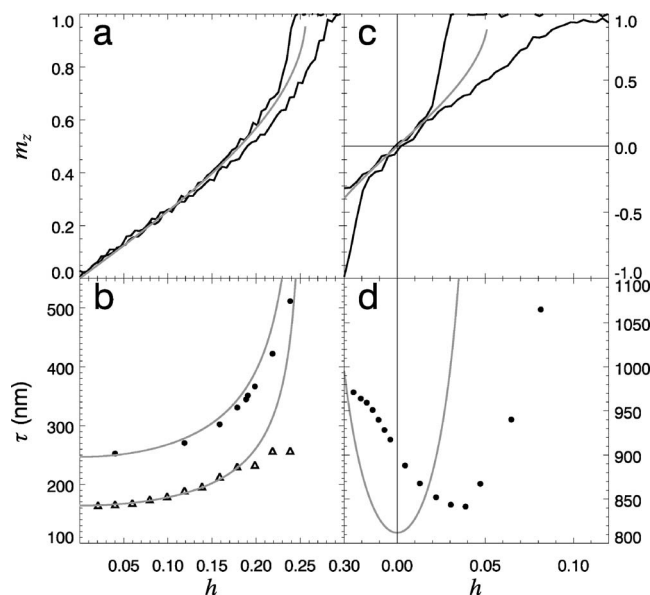


FIG. 8. A comparison of the calculated (gray lines) and measured (black symbols) reduced magnetization (top) and domain period (bottom) versus reduced field from sample A (left) and B (right). Dots and triangles represent, respectively, the disordered and ordered stripes.

than by domain wall pinning. Strictly speaking, the Gehanno description is applicable only to perfectly aligned one-dimensional lattices while the disordered structure is clearly two dimensional. Still, applying a brute force scaling of the calculated period for the aligned case by a factor 1.5 produces a remarkably good agreement with the data.

For sample B, the model gives a magnetization intermediate between the two branches of the hysteresis loop, but clearly is inadequate in describing the field dependence of the average domain distance. The low-saturation magnetization implies much lower dipolar interactions between the up and down domains. This leads to a very large domain period compared to the film thickness ( $\tau/t \approx 22$ ) and a very poor correlation (p. 309 in Ref. 1). Furthermore the large hysteresis in the domain period shows that the dipolar interactions are weak compared to the residual domain pinning. We conclude that in this sample the domain structure is not in the equilibrium state assumed in the continuum model.

## V. CONCLUSIONS

In this paper we discuss a number of aspects of the soft x-ray resonant magnetic scattering technique in the study of nanometer-scale magnetic domain structures, using magnetically striped GdFe thin films as a testing ground. Using the small-angle approximation we explain the origin of the different scattering features in terms of the out-of-plane and the in-plane magnetization components. In particular, we discussed the origin of the circular dichroism in the data of the aligned stripes.

The amount of information that can be extracted from the data depends strongly on the degree of order. In the most

ordered case—the aligned stripes after in-plane saturation—the scattered intensity shows marked circular dichroic asymmetry. At low fields this asymmetry is located at the position of the even diffraction orders, and is the result of interference of the scattering from the out-of-plane and in-plane magnetization components which involve the  $F^{(1)}$  and  $F^{(2)}$  terms of the resonant scattering length. At high fields, the scattering becomes dominated by the form factor of the reversed domains.

The magnitude of the dichroic asymmetry provides a way to estimate the domain wall width. Moreover, the zero crossings of the asymmetry are a direct measure of the reverse domain width which, in combination with the domain period obtained from the peak positions, yields a second independent measure of the absolute value of the magnetization. This value turns out to be in quite good agreement with the magnetization obtained from VSM measurements.

Furthermore, application of Parseval's theorem yields a general relation between the scattered intensity and the expectation value of the modulus of the magnetization, under the condition that the volume of domain walls and closure domains is small. This agreement is observable also in related studies.

Under an applied field, the aligned domains remain parallel to each other up to the field at which they collapse into bubbles. In this case, the magnetization and domain period evolve as predicted by the domain theory of Gehanno *et al.*<sup>31</sup> This is in marked contrast to what was found in XRMS experiments on aligned stripes in Co/Pt multilayered films, where the magnetization adapted to the field by annihilating stripes, leaving surrounding stripes at the same position.<sup>13</sup> We ascribe the differences between the two studies to the fact that the Co/Pt films have a more polycrystalline structure, whereas the amorphous GdFe films studied here were flat and structurally homogeneous on the nanometer scale. Clearly, in films with such a low level of defects, domain theory is valid.

In conclusion, XRMS experiments provide detailed ensemble-averaged information on the evolution of the internal structure of magnetic stripe domains on nanometer-length scales under applied fields. The amount of information extractable substantially increases with the degree of alignment of the stripes. Looking ahead to future possibilities, we note that the use of angular-dependent measurements over a wider  $q$  range together with the exploitation of linear polarization should allow the tomographic reconstruction of the full three-dimensional magnetic structure, which would represent a great step forward in our ability to investigate magnetic systems, both in terms of fundamental insight, as well as technological application.

## ACKNOWLEDGMENTS

The work described in this paper was carried out partly at the European Synchrotron Radiation Facility (Grenoble, France) and is part of the research program of the Stichting voor Fundamenteel Onderzoek der Materie (FOM, Program 39) which is financially supported by the Nederlandse

Organisatie voor Wetenschappelijk Onderzoek (NWO). We thank Huib Luigjes and the WZI workshop for their technical support. We also greatly thank J. Camarero, J. Vogel, and S. Pizzini for their help in the measurements, and M. S. Golden

for a critical reading of the manuscript. J.M. thanks ESRF for the hospitality during his stay there. In particular we wish to remember here the help and support from the late Kenneth Larsson (ESRF).

\*Present address: Institut für Experimentalphysik, Freie Universität Berlin, D-14195 Berlin, Germany. Electronic address: miguel@physik.fu-berlin.de

†Present address: Philips Medical Systems, P.O. Box 10.000, 5680 DA Best, The Netherlands.

‡Present address: ICMCB, UPR 9048 CNRS, Université Bordeaux I, 87 Avenue Dr. A. Schweitzer, 33608 Pessac, France.

§Present address: Diamond Light Source, Chilton, Didcot, Oxfordshire OX11 0QX, United Kingdom.

<sup>1</sup>A. Hubert and R. Schäfer, *Magnetic Domains: The Analysis of Magnetic Microstructures* (Springer, New York, 1998).

<sup>2</sup>P. Fischer, T. Eimüller, G. Schütz, and G. Denbeaux, *Struct. Chem.* **14**, 39 (2003).

<sup>3</sup>T. Eimüller, P. Fischer, M. Köhler, M. Scholz, P. Guttmann, G. Denbeaux, S. Glück, G. Bayreuther, G. Schmahl, D. Attwood *et al.*, *Appl. Phys. A: Mater. Sci. Process.* **73**, 697 (2001).

<sup>4</sup>M. Köhler, J. Zweck, G. Bayreuther, P. Fischer, G. Schütz, G. Denbeaux, and D. Attwood, *J. Magn. Magn. Mater.* **240**, 79 (2002).

<sup>5</sup>F. Nolting, A. Scholl, J. Stöhr, J. W. Seo, J. Fompeyrine, H. Siegwart, J. P. Locquet, S. Anders, J. Lüning, E. E. Fullerton *et al.*, *Nature (London)* **405**, 767 (2000).

<sup>6</sup>H. Ohldag, A. Scholl, F. Nolting, S. Anders, F. U. Hillebrecht, and J. Stöhr, *Phys. Rev. Lett.* **86**, 2878 (2001).

<sup>7</sup>J. Vogel, W. Kuch, M. Bonfim, J. Camarero, Y. Pennec, F. Offi, K. Fukumoto, J. Kirschner, A. Fontaine, and S. Pizzini, *Appl. Phys. Lett.* **82**, 2299 (2003).

<sup>8</sup>W. Kuch, L. I. Chelaru, F. Offi, J. Wang, M. Kotsugi, and J. Kirschner, *Phys. Rev. Lett.* **92**, 017201 (2004).

<sup>9</sup>M. Blume, *J. Appl. Phys.* **57**, 3615 (1985).

<sup>10</sup>E. E. Fullerton, O. Hellwig, K. Takano, and J. B. Kortright, *Nucl. Instrum. Methods Phys. Res. B* **200**, 202 (2003).

<sup>11</sup>H. A. Dürr, E. Dudzik, S. S. Dhesi, J. B. Goedkoop, G. van der Laan, M. Belakhovsky, C. Mocuta, A. Marty, and Y. Samson, *Science* **284**, 2166 (1999).

<sup>12</sup>K. Chesnel, M. Belakhovsky, S. Landis, J. C. Toussaint, S. P. Collins, G. van der Laan, E. Dudzik, and S. S. Dhesi, *Phys. Rev. B* **66**, 024435 (2002).

<sup>13</sup>O. Hellwig, G. P. Denbeaux, J. B. Kortright, and E. E. Fullerton, *Physica B* **336**, 136 (2003).

<sup>14</sup>D. Gibbs, D. R. Harshman, E. D. Isaacs, D. B. McWhan, D. Mills, and C. Vettier, *Phys. Rev. Lett.* **61**, 1241 (1988).

<sup>15</sup>J. P. Hannon, G. T. Trammell, M. Blume, and D. Gibbs, *Phys. Rev. Lett.* **61**, 1245 (1988).

<sup>16</sup>C. Kao, J. B. Hastings, E. D. Johnson, D. P. Siddons, G. C. Smith, and G. A. Prinz, *Phys. Rev. Lett.* **65**, 373 (1990).

<sup>17</sup>C.-C. Kao, C. T. Chen, E. D. Johnson, J. B. Hastings, H. J. Lin, G. H. Ho, G. Meigs, J.-M. Brot, S. L. Hulbert, Y. U. Idzerda *et al.*, *Phys. Rev. B* **50**, 9599 (1994).

<sup>18</sup>J. M. Tonnerre, L. Sève, D. Raoux, G. Soullié, B. Rodmacq, and P. Wolfers, *Phys. Rev. Lett.* **75**, 740 (1995).

<sup>19</sup>J. B. Kortright, S.-K. Kim, G. P. Denbeaux, G. Zeltzer, K. Takano, and E. E. Fullerton, *Phys. Rev. B* **64**, 092401 (2001).

<sup>20</sup>V. Chakarian, Y. U. Idzerda, C.-C. Kao, and C. T. Chen, *J. Magn. Magn. Mater.* **165**, 52 (1997).

<sup>21</sup>C. Schüßler-Langeheine, E. Weschke, A. Y. Grigoriev, H. Ott, R. Meier, D. V. Vyalikh, C. Mazumdar, C. Sutter, D. Abernathy, G. Grübel *et al.*, *J. Electron Spectrosc. Relat. Phenom.* **114**, 953 (2001).

<sup>22</sup>M. Sacchi, C. F. Hague, L. Pasquali, A. Mirone, J.-M. Mariot, P. Isberg, E. M. Gullikson, and J. H. Underwood, *Phys. Rev. Lett.* **81**, 1521 (1998).

<sup>23</sup>S. Eisebitt, M. Lörger, W. Eberhardt, J. Lüning, J. Stöhr, C. T. Rettner, O. Hellwig, E. E. Fullerton, and G. Denbeaux, *Phys. Rev. B* **68**, 104419 (2003).

<sup>24</sup>N. Jaouen, J. M. Tonnerre, D. Raoux, E. Bontempi, L. Ortega, M. Müenzenberg, W. Felsch, A. Rogalev, H. A. Dürr, E. Dudzik *et al.*, *Phys. Rev. B* **66**, 134420 (2002).

<sup>25</sup>E. Dudzik, S. S. Dhesi, H. A. Dürr, S. P. Collins, M. D. Roper, G. van der Laan, K. Chesnel, M. Belakhovsky, A. Marty, and Y. Samson, *Phys. Rev. B* **62**, 5779 (2000).

<sup>26</sup>C. Kooy and U. Enz, *Philips Res. Rep.* **15**, 7 (1960).

<sup>27</sup>A. Marty, Y. Samson, B. Gilles, M. Belakhovsky, E. Dudzik, H. Dürr, S. S. Dhesi, G. van der Laan, and J. B. Goedkoop, *J. Appl. Phys.* **87**, 5472 (2000).

<sup>28</sup>A. Lisfi and J. C. Lodder, *J. Phys.: Condens. Matter* **14**, 12339 (2002).

<sup>29</sup>M. Labrune and J. Miltat, *J. Appl. Phys.* **75**, 2156 (1994).

<sup>30</sup>W. F. Druyvesteyn, J. W. F. Dorleijn, and P. J. Rijnierse, *J. Appl. Phys.* **44**, 2397 (1973).

<sup>31</sup>V. Gehanno, Y. Samson, A. Marty, B. Gilles, and A. Chamberod, *J. Magn. Magn. Mater.* **172**, 26 (1997).

<sup>32</sup>J. A. Cape and G. W. Lehman, *J. Appl. Phys.* **42**, 5732 (1971).

<sup>33</sup>M. Belliard, J. Miltat, V. Kottler, V. Mathet, C. Chappert, and T. Valet, *J. Appl. Phys.* **81**, 5315 (1997).

<sup>34</sup>C. Kittel, *Phys. Rev.* **70**, 965 (1946).

<sup>35</sup>B. Kaplan and G. A. Gehring, *J. Magn. Magn. Mater.* **128**, 111 (1993).

<sup>36</sup><http://math.nist.gov/oommf/>

<sup>37</sup>M. Labrune and J. Miltat, *IEEE Trans. Magn.* **26**, 1521 (1990).

<sup>38</sup>P. Hansen, in *Handbook of Magnetic Materials*, edited by K. H. J. Buschow (North-Holland, 1991), Vol. 6.

<sup>39</sup>H. Fu, M. Mansuripur, and P. Meystre, *Phys. Rev. Lett.* **66**, 1086 (1991).

<sup>40</sup>M. Mansuripur, *The Physical Principles of Magneto-optical Recording* (Cambridge University Press, 1995).

<sup>41</sup>B. T. Thole, G. van der Laan, J. C. Fuggle, G. A. Sawatzky, R. C. Karnatak, and J.-M. Esteve, *Phys. Rev. B* **32**, 5107 (1985).

<sup>42</sup>[http://www.esrf.fr/exp\\_facilities/id8/id8.html](http://www.esrf.fr/exp_facilities/id8/id8.html)

<sup>43</sup>J. F. Peters, M. A. de Vries, J. Miguel, O. Toulemonde, and J. B. Goedkoop, *Eur. Synchro. Rad. Facility Newsletter* **34**, 15 (2000).

- <sup>44</sup>O. Hellwig, S. Maat, J. B. Kortright, and E. E. Fullerton, *Phys. Rev. B* **65**, 144418 (2002).
- <sup>45</sup>E. E. Fullerton, I. K. Schuller, H. Vanderstraeten, and Y. Bruynseraede, *Phys. Rev. B* **45**, 9292 (1992).
- <sup>46</sup>J. P. Hill and D. F. McMorrow, *Acta Crystallogr., Sect. A: Found. Crystallogr.* **52**, 236 (1996).
- <sup>47</sup>J. F. Peters, J. Miguel, M. A. de Vries, O. M. Toulemonde, J. B. Goedkoop, S. S. Dhesi, and N. B. Brookes, *Phys. Rev. B* **70**, 224417 (2004).
- <sup>48</sup>A. W. Rushforth, P. C. Main, B. L. Gallagher, C. H. Marrows, B. J. Hickey, E. D. Dahlberg, and P. Eames, *J. Appl. Phys.* **89**, 7534 (2001).